water

MDPI

Article

Simulation of Seawater Intrusion Area Using Feedforward Neural Network in Longkou, China

Daiyuan Li [1,2,3], Yongxiang Wu [1,2,*], Erkun Gao [2], Gaoxu Wang [1,2], Yi Xu [1,2], Huaping Zhong [1,2] and Wei Wu [1,2]

1 State Key Laboratory of Hydrology-Water Resources and Hydraulic Engineering, Nanjing 210029, China; dyli@nhri.cn (D.L.); gxwang@nhri.cn (G.W.); xuyi@nhri.cn (Y.X.); hpzhong@nhri.cn (H.Z.); wwu@nhri.cn (W.W.)
2 Hydrology and Water Resources Department, Nanjing Hydraulic Research Institute, Nanjing 210029, China; erkgao@mwr.gov.cn
3 College of Hydrology and Water Resource, Hohai University, Nanjing 210098, China
* Correspondence: yxwu@nhri.cn

Received: 7 June 2020; Accepted: 20 July 2020; Published: 24 July 2020

Abstract: Reliable simulation of seawater intrusion (SI) is necessary for sustainable groundwater utilization. As a powerful tool, feedforward neural network (FNN) was applied to study seawater intrusion area (SIA) fluctuations in Longkou, China. In the present study, changes of groundwater level (GWL) were modeled by FNN Model 1. Then, FNN Model 2 was developed for fitting the relationship between GWL and SIA. Finally, two models were integrated to simulate SIA changes in response to climatic and artificial factors. The sensitivity analysis of each impact factor was conducted by the "stepwise" method to quantify the relative importance for SIA and GWL. The results from the integrated model indicated that this method could accurately reproduce SIA fluctuations when the Nash–Sutcliffe efficiency coefficient was 0.964, the root mean square error was 1.052 km^2, the correlation coefficient was 0.983, and the mean absolute error was 0.782 km^2. The results of sensitivity analysis prove that precipitation and groundwater pumping for agriculture mainly affect fluctuations of SIA in the study area. It can be concluded that FNN is effectively used for modeling SI fluctuations together with GWL, which can provide enough support for the sustainable management of groundwater resources with consideration of crucial impact factors of seawater intrusion (SI).

Keywords: seawater intrusion area; simulation; feedforward neural network; sensitivity analysis

1. Introduction

Groundwater is easily accessible freshwater and an essential resource for domestic, agricultural, and industrial purposes in coastal regions. With the rapid growth of human settlements and social economy, these water demands increase the pressure on aquifer, and overexploitation of groundwater resources has become an unavoidable problem in many coastal regions [1,2]. The excessive and unregular exploitation from the coastal aquifer, hydraulically connected with sea, may cause seawater intrusion (SI) [1,3], which seriously threatens the sustainability of groundwater utilization and ecosystems. SI in different areas of the world has been reported in many researches and has obviously become a global issue [2,4–7].

In China, SI was founded as early as the 1960s, and the area was more than 2000 km^2 in 2003 [8]. Longkou, like most coastal areas, has been continuously threatened by SI due to the overexploitation of groundwater resources in the past five decades [8,9]. However, only a handful of previous studies paid attention to it. Wu et al. built a three-dimensional seawater intrusion observation network to provide insight on the characteristics of SI [10]. Xue et al. presented a three-dimensional miscible transport

model considering many important factors, such as variable density on fluid flow, precipitation infiltration, and great discharge pumping wells [11]. Miao et al. built a three-dimensional (3D) variable-density mathematical SI model using SEAWAT and proposed a Kriging surrogate model [12]. As we all know, the SI simulation is necessary for water managers to optimize groundwater utilization and make effective strategies for recovery and prevention of SI. This paper tries to simulate SI changes and identify controlling factors in Longkou by a simulation model, which will be helpful for SI management.

SI, as well as groundwater level (GWL), is generally affected by natural and anthropogenic factors, such as precipitation, surface water level, groundwater pumping, and artificial recharge [13]. Most of the previous researches focused on chloride concentration changes, which are an important indicator to directly represent SI process [2,11,12]. However, the chloride concentrations at some points are not stable and often have the extreme value from monitoring or simulation, which can increase the uncertainty in SI management. To accurately predict SI developing trends, there is a need for monitor station networks with wide distribution and high density. Besides, the chloride concentration monitoring of groundwater is quite expensive. As an alternative, fluctuations of seawater intrusion area (SIA) can be explored to represent SI process in this study, which might provide an easier and more straightforward tool for coastal water management.

During the past several years, conceptual and physically based numerical models were successfully applied to SI simulation in various conditions. Several numerical models such as SEAWAT [12,14–16], FEFLOW [17,18], HYDROGEOSPHERE [19,20], and MOCDENS3D [21–23] have been widely used. Although numerical models have a good performance in many cases, these methods require a large amount of data and many parameters describing the groundwater system and physical properties for the governing equation of groundwater flow and solute transport [24]. It is generally known that a groundwater system is a highly complex and nonlinear system. Thus, a great quantity of data can cause tremendous computational burden and an increase in model uncertainty [25]. Hence, the adaptability of numerical models is poor due to the lack of abundant hydrogeological information. Fortunately, the artificial neural network (ANN) is a strong tool for dealing with the complicated and uncertain system, which demands only time series data for input variables without fully understanding physical or hydrogeological properties [24,26,27].

Although ANN has some drawbacks such as overfitting and risk of using unrelated data, the features including simplicity of use and high-speed run with acceptable accuracy have led many researchers to apply it [28–35]. ANNs can be also developed as surrogate models to approximate complex numerical variable density models [14,26,36–39]. This study focused on the application of the feedforward neural network (FNN) in SIA simulation, which is a typical and frequently used ANN structure. FNN has been widely and successfully used in the hydrological field, such as in the estimation and prediction of streamflow [40–42], water quality [43], and groundwater level [44–46].

The objectives of the study are to evaluate the feasibility of the FNN in SIA simulation and to identify which factors are crucial for SI management. In this paper, FNN models were developed to simulate SIA changes together with GWL in a shallow coastal aquifer. The sensitivity analysis of each impact factor was conducted by the "stepwise" method to quantify the relative importance for SIA and GWL.

2. Materials and Methods

2.1. Study Area and Data

The study area is located at Longkou, Shandong Province, China, which lies between 120°13′14″ to 120°44′46″ east longitude and 37°27′30″ to 37°47′24″ north latitude (Figure 1). The Longkou is a county-level administrative region, whose population is about 718,000. As shown in Figure 1c, there are three key reservoirs, named Wangwu, Chijiagou, and Beixingjia. The red frame area in Figure 1c shows that the main groundwater aquifer, composed of layer Quaternary loose sediment, is situated at the

northern plain of Longkou in terms of the results of the hydrogeological investigation. The study area is approximately 600 km^2, which is approximately 67% of the Longkou, and the total length of the coastline is 68.38 km. As a semihumid monsoon continental climate area, the annual average rainfall is around 594.1 mm (years 1955–2017), out of that 73% occurs from June to September. The annual mean temperature is around 11.8 °C, and the maximum and minimum temperatures are 38.3 °C and −21.3 °C, respectively.

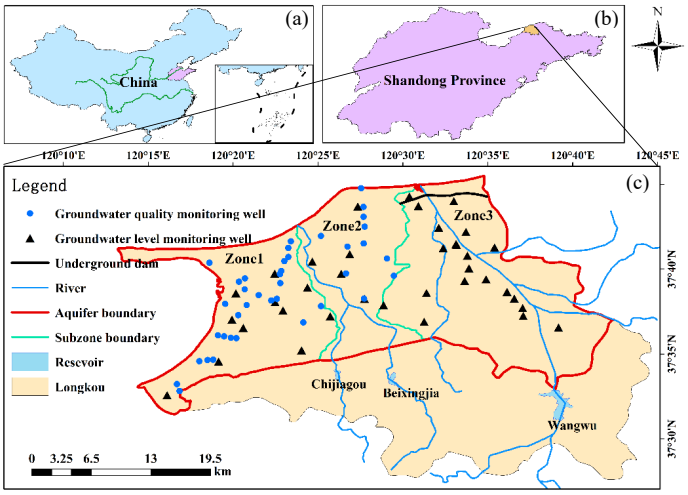

Figure 1. (**a**) Location of Shandong Province in China; (**b**) location of Longkou in Shandong Province; (**c**) description of the study area.

In 1979, SI was first found in the Longkou. From the 1980s to the early 21st century, the amount of groundwater exploitation has been steadily increased in order to cope with the substantial growth of water resource demand. Gradually, SI developed from patches to strips, which posed a severe threat to sustainable development of the social economy and protection of the ecological environment. In order to gain insight on the SI process, the Longkou government made an effort to monitor GWL and groundwater quality, which provides much support to the present study. Figure 1c displays the distributions of GWL-monitoring wells and groundwater quality-monitoring wells.

In this study, six-monthly groundwater chloride concentration (years 2005–2017) and the data (years 2000–2017), including monthly average GWL, monthly precipitation (P), and monthly average temperature (T), were collected from the Longkou government. Besides, annual groundwater supply for agriculture (GWSA), annual groundwater supply for nonagriculture (GWSNA), and annual surface water supply for agriculture (SWSA) were obtained from the Longkou Water Resources Bulletin. It is noted that GWSNA is composed of domestic and industrial water supply. Then, the datasets of annual water supply for agriculture were processed into a monthly value based on crop structure, water demand of crop growth period, and distribution of monthly precipitation. The monthly GWSNA was calculated by the average distribution of annual value.

In addition, according to the hydrogeological data and management demand, the study area was divided into three zones of water resources management (Figure 1c), named Zone1, Zone2, and Zone3. Figure 2 illustrates the changes of monthly average GWL in the three zones. It is apparent that GWL changes of the three zones are similar in trend, and there are high fluctuations. Based on the evaluation results of the second national water resources investigation in Longkou, the annual average quantity of total recharge is about 21.49 million cubic meters, 17.71 million cubic meters, and 58.15 million cubic meters in Zone1, Zone2, and Zone3, respectively. Recharge sources of the unconfined aquifer are similar in three zones, which mainly include the infiltration of precipitation, infiltration of agricultural water, infiltration of rivers, and lateral inflow from the southern mountainous area. The proportions of four recharge sources in annual average quantity of total recharge are approximately 43%, 42%, 5%, and 10% in Zone1; 43%, 37%, 8%, and 10% in Zone2; and 37%, 40%, 17%, and 6% in Zone3.

The discharging sources in Zone1 and Zone2 are primarily composed of groundwater pumping, evaporation, and natural outflow into the sea, in which the annual average quantity of groundwater pumping is about 2.318 million cubic meters, 1.914 million cubic meters, and 5.232 million cubic meters, respectively. However, it is different from Zone1 and Zone2 in that there is no natural outflow into the sea in Zone3, because the underground dam was built 1.2 km from the estuary in 1994 (Figure 1), which completely blocks the hydraulic connection between sea and groundwater system.

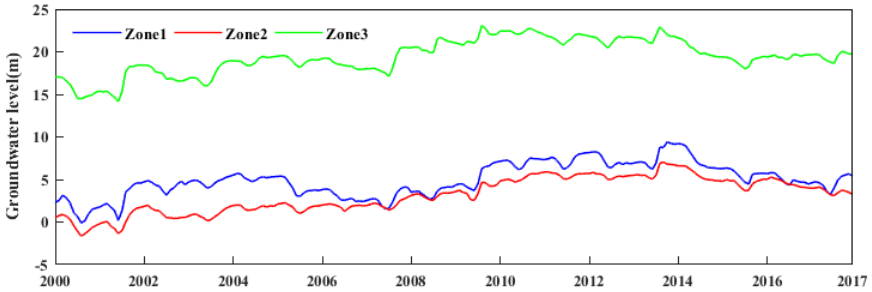

Figure 2. Changes of monthly average groundwater level (GWL) in three zones (years 2000–2017).

The SIA, where the chloride concentration is more than 250 mg/L, was acquired by inverse distance weight interpolation (IDW) of chloride concentration of monitoring wells. It is noted that the area where the chloride concentration is more than 250 mg/L in Zone3 does not need to be considered in the simulative model because of the underground dam. In other words, the GWL drawdown can not make seawater move into land in Zone3. Hence, the SIA referred to the total area of Zone1 and Zone2, which was modeled in this study. As shown in Figure 3, SIA was relieved from 134.4 km^2 in December 2007 to 115.3 km^2 in June 2011, but it showed an increasing trend from 2013 to 2017. Therefore, accurate SIA simulation is very significant for the Longkou government to prevent SI from exacerbating.

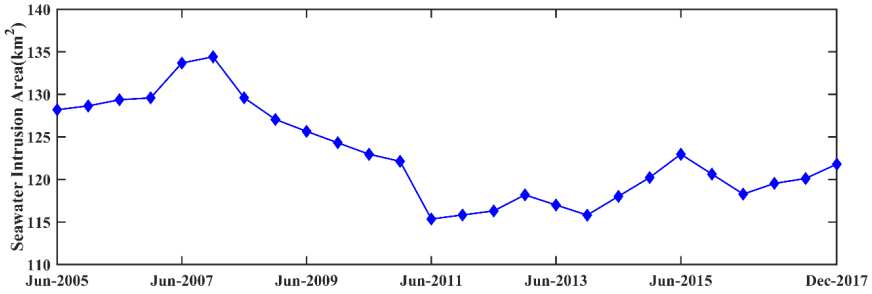

Figure 3. Changes of six-monthly seawater intrusion area (SIA) in the study area (years 2005–2017).

2.2. Feedforward Neural Network

ANN is distributed parallel processors imitating the structure and operation of the human brain [13]. It seems to be a "black" model or empirical model and has self-organization, self-learning, and strong nonlinear ability. The FNN, which is a typical ANN architecture, has been widely applied to kinds of hydrological research. A common FNN is composed of three separate layers, namely, input, hidden, and output layers, each consisting of processing neurons, with interconnections occurring between neurons in adjacent layers.

Figure 4 shows a typical three-layer FNN architecture. The number of neurons in input layers, as well as in output layers, is determined by input variables and targets of the building model. The number of hidden layers is chosen for the best simulation result. Each processing node is interconnected across layers by special nonlinear transfer functions, which means the state of neurons of each layer only has an impact on neurons of the next layers. The distinguishing feature of FNN is the forward propagation of input signals and the backward propagation of the error. During the

training stage, the connection weights and bias are adjusted repeatedly until a minimum acceptable error between simulation and observation is achieved. The mathematical expression of output is given by Equation (1).

$$y_k = f_o\left(\sum_{j=1}^{m} w_{jk} \times f_h\left(\sum_{i=1}^{n} w_{ij} X_i + b_j\right) + b_k\right) \quad (1)$$

where i, j, and k refer to the ith input node, the jth hidden node, and the kth output node, respectively. n and m are the number of input nodes and hidden nodes. w and b represent the weight and the bias. f_h and f_o are the activation functions of hidden layers and output layers. X and y represent the input and output value.

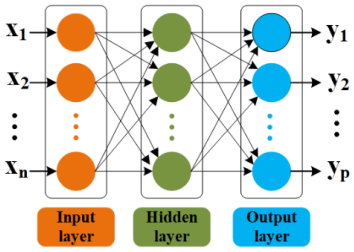

Figure 4. Basic architecture of feedforward neural network with three layers.

A variety of components need to be considered in order to build an appropriate FNN model, including the selection of input variables, the number of hidden layers and nodes, the transfer function of hidden layers and output layers, training algorithm, and criteria of model performance.

The selection of input variables is one of the most important steps in the FNN development. It is noted that not all of the potential input variables will be equally informative because some may be uncorrelated, noisy, or have no significant relationship with the output of models [47]. Commonly, initial input variables are decided based on a priori knowledge about system fundamental properties. Some researches employed a cross-correlation method to reveal linear dependence between two variable time series. Unfortunately, most of the relationship between two variables in the natural groundwater system is nonlinear. In this study, a combination of the priori knowledge and correlation coefficient method was used for determining appropriate input variables.

The activation function is vital to the network, which makes neurons have the ability of perception. The tan-sigmoid function was applied to hidden layers and output layers and is described as Equation (2).

$$f(x) = \frac{2}{(1 + e^{-2x}) - 1} \quad (2)$$

Levenberg–Marquardt algorithm (LM) was applied to train FNN models in the present study, which is a widely popular training algorithm [18]. LM algorithm is a modification of the Newton algorithm for finding an optimal solution about the minimization problem. It has great computational and memory requirements [34], and is faster and less easily trapped in local minima than other optimization algorithms.

In addition, one hidden layer FNN was used, and the number of hidden nodes was also determined by a trial-and-error procedure.

The model performance was evaluated by statistical parameters involving Nash–Sutcliffe efficiency coefficient (E), root mean squared error (RMSE), correlation coefficient (R), and mean absolute error (MAE). The four statistical indicators are defined as follows:

$$\mathrm{E} = 1 - \frac{\sum_{t=1}^{n} (h_{ot} - h_{ct})^2}{\sum_{t=1}^{n} (h_{ot} - \bar{h}_{ot})^2} \quad (3)$$

$$\mathrm{RMSE} = \sqrt{\frac{1}{n}\sum_{t=1}^{n}(h_{ot} - h_{ct})^2} \tag{4}$$

$$\mathrm{R} = \frac{\sum_{t=1}^{n}(h_{ot} - \overline{h}_{ot})(h_{ct} - \overline{h}_{ct})}{\sqrt{\sum_{t=1}^{n}(h_{ot} - \overline{h}_{ot})^2 (h_{ct} - \overline{h}_{ct})^2}} \tag{5}$$

$$\mathrm{MAE} = \frac{1}{n}\sum_{t=1}^{n}|h_{ot} - h_{ct}| \tag{6}$$

where h_{ct} and h_{ot} are simulated and observed values at time t, $\overline{h}_{ct}$ and $\overline{h}_{ot}$ are the average of simulated and observed output series, respectively. The closer that RMSE and MAE are to 0, and E and R are to 1, the better simulations match to observations.

2.3. Application for Seawater Intrusion Area Simulation

SI is caused by the comprehensive function of seawater system and coastal groundwater system. Unregulated and excessive exploitation of groundwater is a primary factor in many coastal regions. The GWL changes provide a direct measure of groundwater development, and SIA can display the degree of SI. Besides, critical information about aquifer dynamics is often embedded in the continuously recorded time series. In this paper, changes of SIA together with GWL were simulated based on FNN, and Figure 5 depicts the model structure, in which n represents the number of input variables. The steps of the model are as follows:

1. The FNN Model 1 is built to simulate GWL changes effected by climatic factors and human activities.
2. The FNN Model 2 is developed to simulate the relationship between GWL of three zones and SIA.
3. FNN Model 1 and FNN Model 2 are integrated, which means that the results of the FNN Model 1 are viewed as the input data of the FNN Model 2. The integrated model can help managers understand SIA changes in response to natural and artificial factors.
4. The sensitivity of each factor is studied by the "stepwise" method, in which input variables are deleted one at a time and the corresponding model is developed and validated. Then, the relative importance ranks are obtained by comparison of model performance criteria, and crucial impact factors are identified for SIA and GWL.

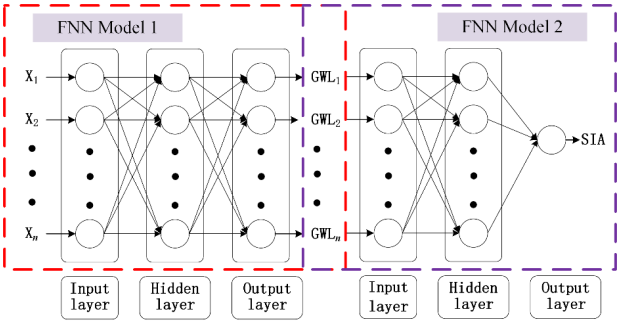

Figure 5. Configuration of the model for SIA simulation.

3. Results and Discussion

3.1. Groundwater Level Simulation

3.1.1. Determination of FNN Model 1 Architecture

As aforementioned, the determination of model architecture should be learned from the fundamental conceptual knowledge of the study area. According to the water budget description of the aquifer in Section 2.1, the major influence factors include infiltration of precipitation, infiltration of agricultural water, groundwater exploitation, and evaporation. It is noted that the influence of lateral inflow and outflow into sea for the groundwater system was not considered because the quantity is so small that they have a weak impact on GWL. The infiltration of rivers was likewise ignored in the model due to the long drying-out of rivers. Besides, the evaporation of groundwater system is extremely difficult to quantify over space and time. As an alternative, the monthly average temperature was considered as an input variable in this model. In the study area, there is a combination of surface water utilization from water storage projects and groundwater pumping for irrigation. When the total amount of groundwater and surface water for irrigation is constant, the response of groundwater system is obviously different. This is because GWSA is both a discharge and a recharge resource and SWSA is only a recharge resource. According to whether it can feed the aquifer, groundwater exploitation was divided into GWSA and GWSNA. Also, the initial monthly average GWL was considered as a fundamental input.

It should be noted that different time lags of factors for model performance were considered. Different lengths of precipitation, temperature, GWSA, GWSNA, and SWSA varying from 1 to 6 months were tested by the trial-and-error method. It was found that the delay contribution of factors, except precipitation, had no positive effect on model performance, and one time-lag of precipitation had an optimal performance. The autocorrelation coefficients for identifying appropriated lengths of GWL time-lag of three zones from 1 to 6 months are given in Table 1. One time-lag was highly significant with autocorrelation coefficients of 0.975, 0.990, and 0.981 in three zones, respectively.

Table 1. Autocorrelation coefficients of monthly average GWL in three zones.

Time-Lag	Zone1	Zone2	Zone3
$t-1$	0.975	0.990	0.981
$t-2$	0.927	0.969	0.944
$t-3$	0.879	0.948	0.910
$t-4$	0.839	0.931	0.882
$t-5$	0.812	0.919	0.858
$t-6$	0.790	0.910	0.838

Note: t represents the monthly time step of feedforward neural network (FNN) Model 1.

In summary, input variables of FNN Model 1 included monthly precipitation at time t (P(t)), monthly precipitation at time $t-1$ (P($t-1$)), monthly average temperature at time t (T(t)), monthly groundwater supply for agriculture at time t (GWSA(t)), monthly groundwater supply for nonagriculture at time t (GWSNA(t)), monthly surface water supply for agriculture at time t (SWSA(t)), monthly average GWL of Zone1 at time $t-1$ ($GWL_1(t-1)$), monthly average GWL of Zone2 at time $t-1$ ($GWL_2(t-1)$), and monthly average GWL of Zone3 at time $t-1$ ($GWL_3(t-1)$). It is noted that t represents the monthly time step of FNN Model 1.

Output variables of FNN Model 1 included monthly average GWL of Zone1 at time t ($GWL_1(t)$), monthly average GWL of Zone2 at time t ($GWL_2(t)$), and monthly average GWL of Zone3 at time t ($GWL_3(t)$). The datasets were separated into two different parts. For the training set, 80% of the collected and preprocessed data were used, and 20% were used for the validation set. The activation function of hidden layers and output layers, the number of hidden layers, and the training algorithm in FNN Model 1 are described in Section 2.2. The number of nodes in the hidden layer was determined

by the trial-and-error method. The trial-and-error procedure started with five hidden neurons initially, and the number of hidden neurons was increased to twenty. The optimum number of hidden neurons was found to be ten.

3.1.2. Results of FNN Model 1

Figure 6 depicts the monthly average GWL simulation of three zones for the validation stage (July 2014–December 2017). It is noted that the blue line represents the observed GWL, and the red line represents the simulated GWL in Figure 6a–c. These figures indicate that there was a good fitting between observation and simulation in three zones. The performances of FNN Model 1 in terms of E, RMSE, R, and MAE are presented in Table 2. It is apparent from this table that during the validation period, E value varied from 0.908 to 0.997, RMSE value varied from 0.133 m to 0.251 m, R value varied from 0.965 to 0.998, and MAE value varied from 0.100 m to 0.184 m. Hence, FNN Model 1 has the ability to model GWL fluctuations with reasonable accuracy, which can help managers obtain more information on the groundwater system to enhance groundwater resource management.

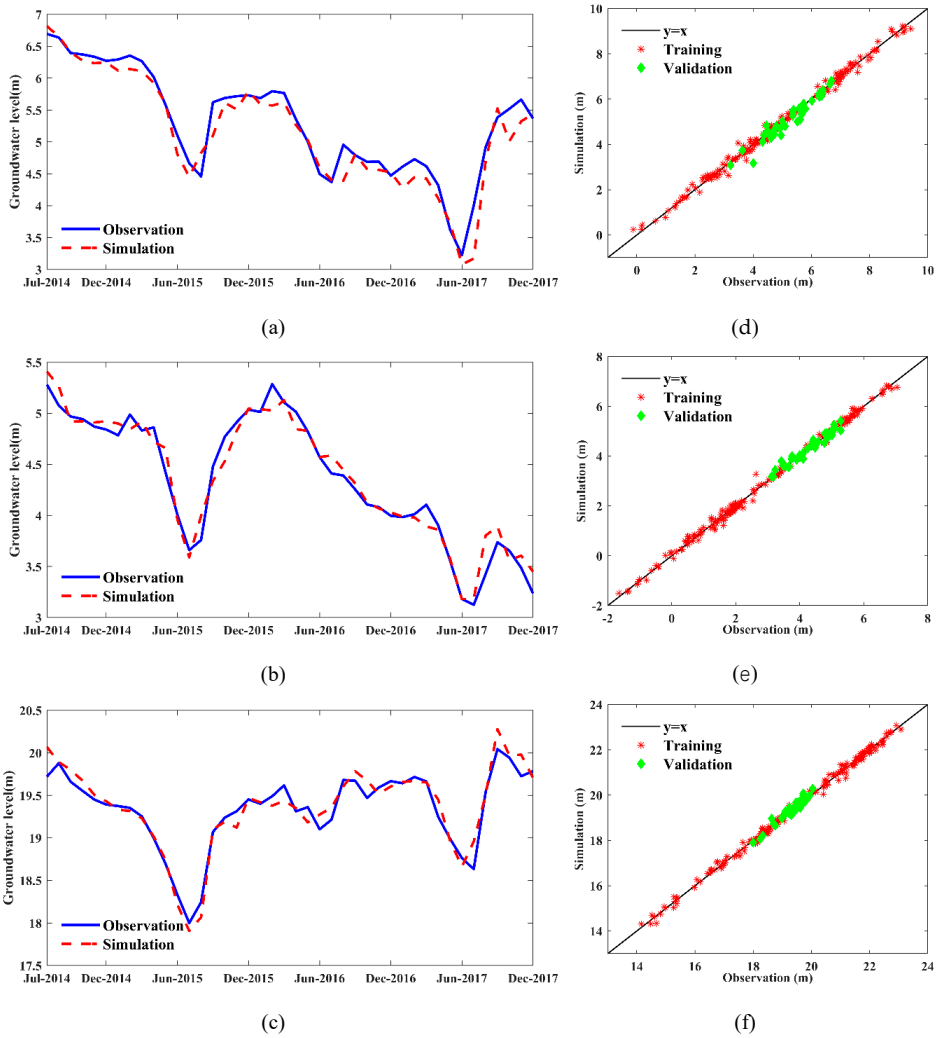

Figure 6. Comparison between observation and simulation of monthly average GWL using FNN Model 1: (**a–c**) Line plot of results in Zone1, Zone2, and Zone3 during validation period, respectively; (**d–f**) Scatter plot of results in Zone1, Zone2, and Zone3 during training and validation period, respectively.

Table 2. Statistical indicators of FNN Model 1 performance during training and validation period.

Zone	Period	E	RMSE (m)	R	MAE (m)
Zone1	Training	0.994	0.169	0.997	0.127
	Validation	0.908	0.251	0.970	0.184
Zone2	Training	0.996	0.133	0.998	0.100
	Validation	0.954	0.134	0.977	0.101
Zone3	Training	0.997	0.133	0.998	0.104
	Validation	0.911	0.133	0.965	0.102

The names of abbreviations are described in Table A1.

3.2. Seawater Intrusion Area Simulation

3.2.1. Determination of FNN Model 2 Architecture

Seawater intrusion means that the balanced interface between groundwater system and seawater system moves to land. In the study area, the correlation coefficient between six-monthly average sea level and six-monthly SIA was about −0.179, which indicated that variations of sea level have a little influence on SIA fluctuations during the simulated period (years 2005–2017). Therefore, this section pays attention to the relationship between GWL and SIA. In FNN Model 2, the six-monthly average GWL of three zones and initial SIA were considered in the input layer. Correlation coefficients between GWL of each zone and SIA are presented in Table 3. Further, different lengths of GWL varying from 0 to 6 time steps were tested by the trial-and-error method. Altogether, it was found that time lag > 1 of GWL in each zone does not provide a significant contribution to the model performance. In short, input variables of FNN Model 2 included $GWL_1(k)$, $GWL_1(k-1)$, $GWL_2(k)$, $GWL_2(k-1)$, $GWL_3(k)$, and $GWL_3(k-1)$. It should be noted that k represents the six-monthly time step of FNN Model 2. The output variable only included SIA at time k. In addition, datasets were divided into two different parts—80% of the collected data were viewed as the training set; the other 20% for the validation set.

Table 3. The correlation coefficient between GWL of three zones and SIA, respectively.

Time-Lag	Zone1	Zone2	Zone3
k	0.845	0.896	0.543
$k-1$	0.831	0.910	0.681
$k-2$	0.770	0.875	0.724
$k-3$	0.705	0.834	0.747
$k-4$	0.601	0.799	0.746
$k-5$	0.463	0.754	0.759
$k-6$	0.304	0.699	0.760

Note: k represents the six-monthly time step of FNN Model 2.

In FNN Model 2, the activation function of hidden layers and output layers, the number of hidden layers, and the training algorithm are described in Section 2.2, as well as FNN Model 1. The number of hidden neurons in the network was identified by various trials. The trial-and-error procedure started with two hidden neurons initially, and the number of hidden neurons was increased to twenty. It was found that thirteen neurons were optimal for model performance.

3.2.2. Results of FNN Model 2

Figure 7 presents the simulation of six-monthly SIA by FNN Model 2 for the training and validation period (years 2005–2017). It illustrated that there was a good matching between observation and simulation. The four statistical indicators of model performance are shown in Table 4. It can be seen from the table that during the training, the statistical indicators E, RMSE, R, and MAE were 0.978, 0.877 km^2, 0.990, and 0.575 km^2, respectively, and the corresponding parameters were 0.821, 0.493 km^2, 0.941, and 0.295 km^2 during the validation. The values of statistical indicators implied

that the performance of FNN Model 2 was satisfactory during both the training and the validation period. Overall, the FNN Model 2 is capable of an understanding relationship between SIA and GWL. Meanwhile, the results prove that SIA and GWL are closely related, which is in agreement with the previous research [9].

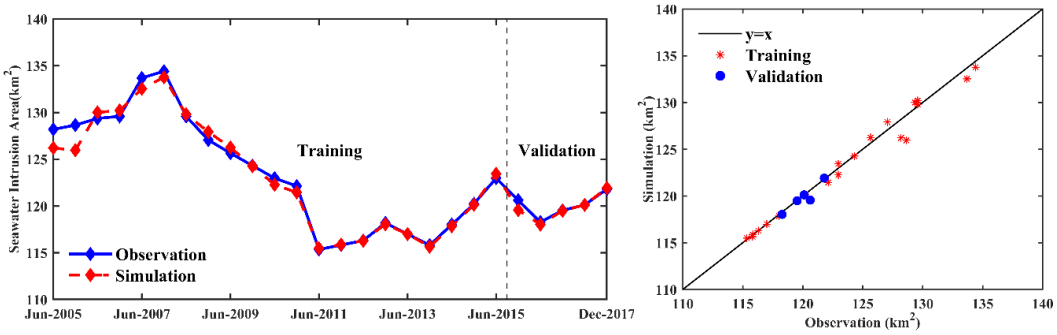

(a) (b)

Figure 7. Comparison between observation and simulation of six-monthly SIA using FNN Model 2: (**a**) line plot of results; (**b**) scatter plot of results.

Table 4. Statistical indicators of FNN Model 2 during the training and validation period.

Period	E	RMSE (km^2)	R	MAE (km^2)
Training	0.978	0.877	0.990	0.575
Validation	0.821	0.493	0.941	0.295

The names of abbreviations are described in Table A1.

3.2.3. Integrated Model

In this section, FNN Model 1 and FNN Model 2 are integrated, which can help managers study the SIA fluctuations in response to water exploitation activities and climate factors. The results of monthly average GWL (years 2005–2017) from FNN Model 1 were processed into six-monthly average GWL, which was considered as input data for FNN Model 2. Figure 8 displays a comparison between simulation and observation, and statistical indicators of model performance for the computation period are shown, in which E scored for 0.964, RMSE scored for 1.052 km^2, R scored for 0.983, and MAE scored for 0.782 km^2. Therefore, the integrated model had an excellent performance based on statistical indicators and graphs, which can be used for accurately predicting SI development.

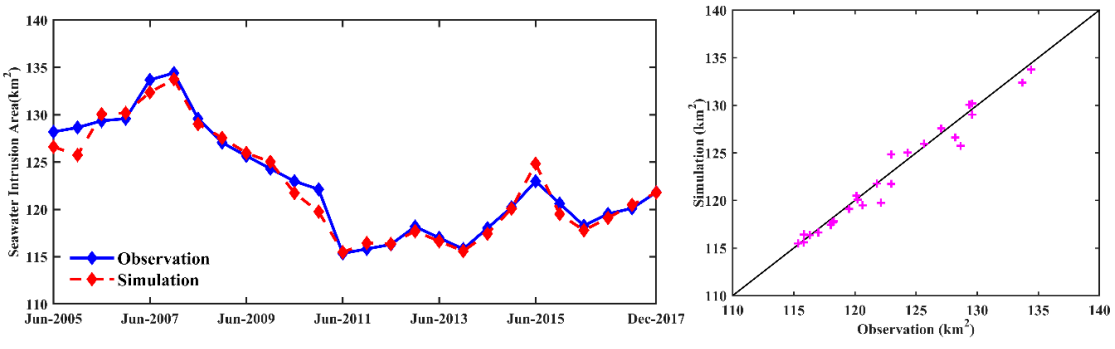

(**a**) (**b**)

Figure 8. Comparison between observation and simulation of six-monthly SIA using integrated model: (**a**) line plot of results; (**b**) scatter plot of results.

3.3. Sensitivity Analysis for GWL and SIA Simulation

After the FNN models for GWL and SIA simulation were developed, one of the significant objectives in this study was to gain a better understanding of natural and anthropogenic factors for the

coastal groundwater system. In other words, the relative importance of each factor for fluctuations of GWL and SIA was analyzed. In this section, the "stepwise" method, in which one input variable was deleted and the corresponding model was developed and validated, is outlined, and statistical indicators of model performance are compared. Based on the input variables set of FNN Model 1 in Section 3.1, six input scenarios for sensitivity analysis were established, which are presented in Table 5. The absolute relative bias of simulation was displayed by a box plot to make a qualitative analysis. The relative importance rank of each factor was obtained based on the ratio, which is described by Equation (7). A ratio value >1 represents that the elimination of the factor reduces the simulative accuracy. Hence, the larger the ratio, the stronger the influence of the missing factor on the target.

$$ratio = \frac{\text{MAE } without \ \ one \ factor \ \ in \ \ input \ \ layer}{\text{MAE } with \ \ all \ \ variables} \tag{7}$$

Table 5. Six input scenarios sets for sensitivity analysis.

No.	Scenarios	Input Variables Set
-	All variables	P(t), P($t-1$), T(t), GWSA(t), GWSNA(t), SWSA(t), $GWL_1(t-1)$, $GWL_2(t-1)$, $GWL_3(t-1)$
1	No-P(t)	P($t-1$), T(t), GWSA(t), GWSNA(t), SWSA(t), $GWL_1(t-1)$, $GWL_2(t-1)$, $GWL_3(t-1)$
2	No-P($t-1$)	P(t), T(t), GWSA(t), GWSNA(t), SWSA(t), $GWL_1(t-1)$, $GWL_2(t-1)$, $GWL_3(t-1)$
3	No-T	P(t), P($t-1$), GWSA(t), GWSNA(t), SWSA(t), $GWL_1(t-1)$, $GWL_2(t-1)$, $GWL_3(t-1)$
4	No-GWSA	P(t), P($t-1$), T(t), GWSNA(t), SWSA(t), $GWL_1(t-1)$, $GWL_2(t-1)$, $GWL_3(t-1)$
5	No-GWSNA	P(t), P($t-1$), T(t), GWSA(t), SWSA(t), $GWL_1(t-1)$, $GWL_2(t-1)$, $GWL_3(t-1)$
6	No-SWSA	P(t), P($t-1$), T(t), GWSA(t), GWSNA(t), $GWL_1(t-1)$, $GWL_2(t-1)$, $GWL_3(t-1)$

The names of abbreviations are described in Table A1.

3.3.1. Sensitivity Analysis for GWL Simulation

The validation period of FNN Model 1 (July 2014–December 2017) was used for sensitivity analysis. Figure 9 illustrates the absolute relative bias distributions of simulation with different scenarios. The relative importance ranks of factors are presented in Table 6. The results of GWL sensitivity analysis showed that natural and anthropogenic variables, except the temperature in Zone1, can improve the capability of FNN Model 1.

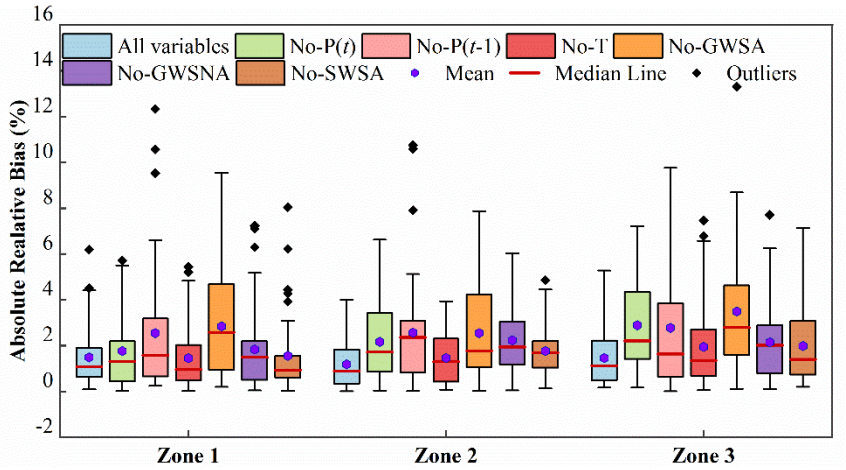

Figure 9. Box plot of absolute relative bias distributions of GWL simulation with different input variables sets in Zone1, Zone2, and Zone3. The ends of boxes represent the first and third quartiles, and the whiskers represent the values at 1.5 standard deviations.

Table 6. The sensitivity analysis results of impact factors for monthly average GWL.

Zone	No.	Scenario	Factor	MAE	Ratio	Rank
Zone1	-	All variables	-	0.184	-	-
	1	No-P(t)	P(t)	0.218	1.185	4
	2	No-P($t-1$)	P($t-1$)	0.313	1.701	2
	3	No-T	T	0.179	0.973	6
	4	No-GWSA	GWSA	0.351	1.908	1
	5	No-GWSNA	GWSNA	0.228	1.239	3
	6	No-SWSA	SWSA	0.191	1.038	5
Zone2	-	All variables	-	0.101	-	-
	1	No-P(t)	P(t)	0.184	1.822	4
	2	No-P($t-1$)	P($t-1$)	0.221	2.188	2
	3	No-T	T	0.125	1.238	6
	4	No-GWSA	GWSA	0.222	2.198	1
	5	No-GWSNA	GWSNA	0.190	1.881	3
	6	No-SWSA	SWSA	0.150	1.485	5
Zone3	-	All variables	-	0.102	-	-
	1	No-P(t)	P(t)	0.201	1.971	2
	2	No-P($t-1$)	P($t-1$)	0.193	1.892	3
	3	No-T	T	0.135	1.324	6
	4	No-GWSA	GWSA	0.243	2.382	1
	5	No-GWSNA	GWSNA	0.149	1.461	4
	6	No-SWSA	SWSA	0.140	1.373	5

The names of abbreviations are described in Table A1.

Figure 9 shows that the median and mean value of absolute relative bias with No-GWSA in all zones were larger than those of the other input scenarios, which demonstrated that GWSA had the greatest impact on the accuracy of GWL simulation among all factors. The same conclusion can be held with the relative importance rank of GWSA. According to the absolute relative bias distributions in Figure 9, the precipitation has more influence on GWL changes than T, GWSNA, and SWSA. However, the relative importance of different time lag of precipitation was not equal in different zones. In Zone1 and Zone2, values of MAE were 0.313 m and 0.221 m, respectively, under the No-P($t-1$) scenario, and were greater than those of the No-P(t) scenario, where values of MAE were 0.218 m and 0.184 m. It was indicated that P($t-1$) is more important than P(t) for GWL simulation in Zone1 and Zone2, but the result was converse in Zone3. It seemed that groundwater depth might influence the recharge rate of precipitation, and the groundwater depth of Zone1 was generally larger than that of the other zones based on the analysis of monitoring data. In addition, it was not surprising that the temperature had minimal influence on model performance, ranked 6th in all zones, and the accuracy of simulation in Zone1 with No-T was even better than that of the scenario of all variables. This is because the groundwater depth is so high that groundwater evaporation is very small, especially in Zone1.

Further structures of water resource utilization can be demonstrated based on results of the sensitivity analysis of artificial factors. As stated by many authors, in semi-arid regions, as surface water resources are scarce, groundwater is heavily pumped to irrigation, which contributes to the rapid deterioration of the groundwater quality [48–50]. In the study, this phenomenon has been confirmed by data analysis in Longkou. It is clearly shown from the absolute relative bias distributions of boxplot (Figure 9) that the contribution of GWSNA for GWL changes was weaker than that of GWSA. It revealed that GWSA constitutes a high proportion in total groundwater consumption, which can be proved by the general survey of groundwater pumping wells in 2011. As expected, the relative importance ranks of SWSA in Zone1, Zone2, and Zone3 were all fifth, which indicated that the contribution of SWSA for GWL fluctuations was the weakest among all artificial factors. The same result is obviously obtained from Figure 9. In Zone1, there are hardly projects of surface water irrigation, and the factor of SWSA has almost no effect on the groundwater system of Zone1. Although the irrigation region of the Wangwu reservoir is located at Zone3, the large reservoir mainly guaranteed domestic and

industrial water supply during the simulative period according to the operational data. The SWSA in the study area is mainly composed of the Chijiagou reservoir and the Beixingjia reservoir in Zone2, which provide some surface water for wheat irrigation from March to May and pumping from rivers in flood season. Hence, the quantity of SWSA is very small.

3.3.2. Sensitivity Analysis for SIA Simulation

Based on FNN models with six scenarios, as outlined in Section 3.3.1, sensitivity of natural and anthropogenic factors for SIA was analyzed by the integrated model. The absolute relative bias distributions of SIA simulation are presented in Figure 10, and the relative importance rank of each factor is obtained in Table 7. As expected, factors of P(t), P($t-1$), and GWSA had more contributions to SIA fluctuations, which ranked third, second, and first, respectively. The same conclusion can be held from the qualitative analysis of Figure 10, and GWSA was the closest to SIA among these factors. In addition, the relative importance of T, GWSNA, and SWSA ranked fifth, fourth, and sixth. This is because groundwater depth is so high that the influence of groundwater evaporation can be ignored. Meanwhile, contributions of GWSNA and SWSA for SIA are affected by groundwater pumping distributions. The irrigation region of surface water at piedmont is far from the coastal line, and the amount of surface water for irrigation is also small. Wu et al. presented that the specific distribution of SI has a relation with the strong pumping center [9]. According to the general survey of groundwater pumping wells in 2011, most of domestic and industrial pumping wells are mainly located in central and south parts of the study area. Therefore, it was not surprising that T, GWSNA, and SWSA were weakly correlated to SIA. The results are consistent with the previous research [51]. It is apparent that strengthening groundwater management for agriculture is significant for solving the SI problem in Longkou.

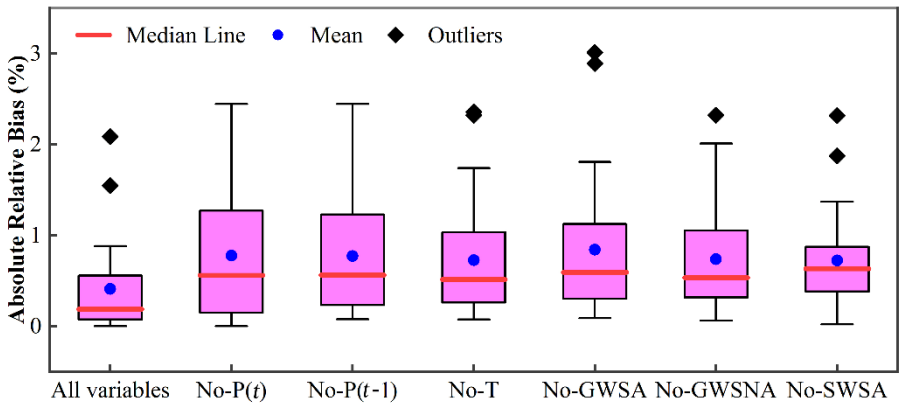

Figure 10. Box plot of absolute relative bias distributions of simulation with different input variables sets; The ends of boxes represent the first and third quartiles, and the whiskers represent the values at 1.5 standard deviations.

Table 7. Sensitivity analysis results of impact factors for six-monthly SIA.

No.	Scenario	Factor	MAE (km^2)	Ratio	Rank
-	All variables	-	0.782	-	-
1	No-P(t)	P(t)	0.961	1.229	3
2	No-P($t-1$)	P($t-1$)	0.962	1.230	2
3	No-T	T	0.909	1.162	5
4	No-GWSA	GWSA	1.043	1.334	1
5	No-GWSNA	GWSNA	0.917	1.173	4
6	No-SWSA	SWSA	0.902	1.153	6

The names of abbreviations are described in Table A1.

4. Conclusions

In this study, FNN was applied to study SIA and GWL of a shallow coastal aquifer in Longkou, Shandong Province, China. The results from the model indicated that this method could accurately reproduce fluctuations of SIA and GWL. It is concluded that FNN is an excellent choice for estimating SI changes together with GWL in the coastal aquifer, even influenced by highly irregular anthropogenic factors. Besides, this paper demonstrates that SIA can be considered as an alternative to estimate the development of SI, which is easier and more direct to use in water management.

According to sensitivity analysis results, GWSA and precipitation have a strong impact on changes of SI and GWL. However, the relative importance of artificial factors for SIA is different from that of GWL. It depends on the distributions of pumping wells. For example, GWSNA had more influence on GWL, especially in Zone1 and Zone2, but the contribution for SIA changes is weak. Hence, when researchers apply artificial neural network models to the groundwater system, the subzone division of study areas should be considered based on the features of water users and physical properties. Meanwhile, this study can alert the government to capture crucial factors and make effective strategies in SI management.

The modeling results and analysis will help decisionmakers gain insight on the influence of human activities on the groundwater system and promote the sustainable use of groundwater resources. In the future, the present work can be extended to develop artificial neural network models to estimate SIA at a monthly time step and identify control factors in different subregions. This work will provide more reasonable support for SI prevention.

Author Contributions: D.L. conducted the research, performed analyses, and wrote the manuscript. Y.W., E.G., G.W., and H.Z. make helpful discussions and provide technical assistance. Y.X. and W.W. revised the manuscript and given some suggestions about the expression of English scientific papers. All authors have read and agreed to the published version of the manuscript.

Funding: This research was funded by the National Key R&D Program of China (No. 2016YFC0402808 and No. 2016YFC0401005). This research was also supported by Nanjing Hydraulic Research Institute Fund (No. Y519014) and Nanjing Hydraulic Research Institute Dissertation Fund (No. LB11904).

Acknowledgments: We much appreciate the Longkou Water-affair Authority for providing the monitoring data and background information of the study area. The authors would like to thank the editors and reviewers for constructive comments that greatly contributed to improving the manuscript.

Conflicts of Interest: The authors declare no conflict of interest.

Appendix A

Table A1. The description of abbreviations in the paper.

No.	Abbreviation	Description
1	E	Nash–Sutcliffe model efficiency coefficient
2	FNN	Feedforward neural network
3	GWL	Groundwater level
4	GWSA	Groundwater supply for agriculture
5	GWSNA	Groundwater supply for nonagriculture
6	IDW	Inverse distance weight interpolation
7	MAE	Mean absolute error
8	P	Precipitation
9	R	Correlation coefficient
10	RMSE	Root mean squared error
11	SI	Seawater intrusion
12	SIA	Seawater intrusion area
13	SWSA	Surface water supply for agriculture
14	T	Temperature

References

1. Bhattacharjya, R.K.; Datta, B.; Satish, M.G. Performance of an Artificial Neural Network model for simulating saltwater intrusion process in coastal aquifers when training with noisy data. *KSCE J. Civ. Eng.* **2009**, *13*, 205–215. [CrossRef]
2. Dey, S.; Prakash, O. Management of Saltwater Intrusion in Coastal Aquifers: An Overview of Recent Advances. In *Environmental Processes and Management*; Springer: Cham, Germany, 2020; pp. 321–344.
3. Giordano, R.; Milella, P.; Portoghese, I.; Vurro, M.; Apollonio, C.; Dagostino, D.; Lamaddalena, N.; Scardigno, A.; Piccinni, A.F. An innovative monitoring system for sustainable management of groundwater resources: Objectives, stakeholder acceptability and implementation strategy. In Proceedings of the Workshop on Environmental Energy and Structural Monitoring Systems, Taranto, Italy, 9 September 2010; pp. 32–37.
4. Werner, A.D.; Bakker, M.; Post, V.E.; Vandenbohede, A.; Lu, C.; Ataie-Ashtiani, B.; Simmons, C.T.; Barry, D.A. Seawater intrusion processes, investigation and management: Recent advances and future challenges. *Adv. Water Resour.* **2013**, *51*, 3–26. [CrossRef]
5. Idowu, T.E.; Lasisi, K.H. Seawater intrusion in the coastal aquifers of East Africa and the Horn of Africa: A review from a regional perspective. *Sci. Afr.* **2020**, *8*, e00402. [CrossRef]
6. Vann, S.; Puttiwongrak, A.; Suteerasak, T.; Koedsin, W. Delineation of Seawater Intrusion Using Geo-Electrical Survey in a Coastal Aquifer of Kamala Beach, Phuket, Thailand. *Water* **2020**, *12*, 506. [CrossRef]
7. Zeynolabedin, A.; Ghiassi, R.; Dolatshahi Pirooz, M. Seawater intrusion vulnerability evaluation and prediction: A case study of Qeshm Island, Iran. *J. Water Clim. Chang.* **2020**, 3–26. [CrossRef]
8. Shi, L.; Jiao, J.J. Seawater intrusion and coastal aquifer management in China: A review. *Environ. Earth Sci.* **2014**, *72*, 2811–2819. [CrossRef]
9. Wu, J.; Meng, F.; Wang, X.; Wang, D. The development and control of the seawater intrusion in the eastern coastal of Laizhou Bay, China. *Environ. Geol.* **2008**, *54*, 1763–1770. [CrossRef]
10. Wu, J.; Xue, Y.; Liu, P.; Wang, J.; Jiang, Q.; Shi, H. Sea-Water Intrusion in the Coastal Area of Laizhou Bay, China: 2. Sea-Water Intrusion Monitoring. *Groundwater* **1993**, *31*, 740–745. [CrossRef]
11. Xue, Y.; Xie, C.; Wu, J.; Liu, P.; Wang, J.; Jiang, Q. A three-dimensional miscible transport model for seawater intrusion in China. *Water Resour. Res.* **1995**, *31*, 903–912. [CrossRef]
12. Miao, T.; Lu, W.; Lin, J.; Guo, J.; Liu, T. Modeling and uncertainty analysis of seawater intrusion in coastal aquifers using a surrogate model: A case study in Longkou, China. *Arab. J. Geosci.* **2019**, *12*, 1. [CrossRef]
13. Lee, S.; Lee, K.K.; Yoon, H. Using artificial neural network models for groundwater level forecasting and assessment of the relative impacts of influencing factors. *Hydrogeol. J.* **2019**, *27*, 567–579. [CrossRef]
14. Rao, S.; Sreenivasulu, V.; Bhallamudi, S.M.; Thandaveswara, B.; Sudheer, K. Planning groundwater development in coastal aquifers/Planification du développement de la ressource en eau souterraine des aquifères côtiers. *Hydrol. Sci. J.* **2004**, *49*, 155–170. [CrossRef]
15. Jin, L.; Snodsmith, J.B.; Zheng, C.; Wu, J. A modeling study of seawater intrusion in Alabama Gulf Coast, USA. *Environ. Geol.* **2009**, *57*, 119–130.
16. Luyun, R.; Momii, K.; Nakagawa, K. Laboratory-scale saltwater behavior due to subsurface cutoff wall. *J. Hydrol.* **2009**, *377*, 227–236. [CrossRef]
17. Gossel, W.; Sefelnasr, A.; Wycisk, P. Modelling of paleo-saltwater intrusion in the northern part of the Nubian Aquifer System, Northeast Africa. *Hydrogeol. J.* **2010**, *18*, 1447–1463. [CrossRef]
18. Watson, T.A.; Werner, A.D.; Simmons, C.T. Transience of seawater intrusion in response to sea level rise. *Water Resour. Res.* **2010**, *46*, W12533. [CrossRef]
19. Graf, T.; Therrien, R. Variable-density groundwater flow and solute transport in porous media containing nonuniform discrete fractures. *Adv. Water Resour.* **2005**, *28*, 1351–1367. [CrossRef]
20. Thompson, C.; Smith, L.; Maji, R. Hydrogeological modeling of submarine groundwater discharge on the continental shelf of Louisiana. *J. Geophys. Res. Ocean.* **2007**, *112*, 1–13. [CrossRef]
21. Bakker, M.; Oude Essink, G.H.P.; Lengevin, C.D. The rotating movement of three immiscible fluids—a benchmark problem. *J. Hydrol.* **2004**, *287*, 270–278. [CrossRef]
22. Vandenbohede, A.; Lebbe, L. Occurrence of salt water above fresh water in dynamic equilibrium in a coastal groundwater flow system near De Panne, Belgium. *Hydrogeol. J.* **2006**, *14*, 462–472. [CrossRef]
23. Oude Essink, G.H.P.; van Baaren, E.S.; de Louw, P.G.B. Effects of climate change on coastal groundwater systems: A modeling study in the Netherlands. *Water Resour. Res.* **2010**, *46*. [CrossRef]

24. Rajaee, T.; Ebrahimi, H.; Nourani, V. A review of the artificial intelligence methods in groundwater level modeling. *J. Hydrol.* **2019**, *572*, 336–351. [CrossRef]
25. Khan, U.T.; Valeo, C. Dissolved oxygen prediction using a possibility theory based fuzzy neural network. *Hydrol. Earth Syst. Sci.* **2016**, *20*, 2267–2293. [CrossRef]
26. Singh, A. Optimization modelling for seawater intrusion management. *J. Hydrol.* **2014**, *508*, 43–52. [CrossRef]
27. Rajaee, T.; Boroumand, A. Forecasting of chlorophyll-a concentrations in South San Francisco Bay using five different models. *Appl. Ocean. Res.* **2015**, *53*, 208–217. [CrossRef]
28. ASCE Task Committee on Application of Artificial Neural Networks in Hydrology. Artificial neural networks in hydrology. II: Hydrologic applications. *J. Hydrol. Eng.* **2000**, *5*, 124–137. [CrossRef]
29. ASCE Task Committee on Application of Artificial Neural Networks in Hydrology. Artificial neural networks in hydrology. I: Preliminary concepts. *J. Hydrol. Eng.* **2000**, *5*, 115–123. [CrossRef]
30. Daliakopoulos, I.N.; Coulibaly, P.; Tsanis, I.K. Groundwater level forecasting using artificial neural networks. *J. Hydrol.* **2005**, *309*, 229–240. [CrossRef]
31. Coppola, E.A., Jr.; Rana, A.J.; Poulton, M.M.; Szidarovszky, F.; Uhl, V.W. A neural network model for predicting aquifer water level elevations. *Groundwater* **2010**, *43*, 231–241.
32. Jha, M.K.; Sahoo, S. Efficacy of neural network and genetic algorithm techniques in simulating spatio-temporal fluctuations of groundwater. *Hydrol. Process.* **2015**, *29*, 671–691. [CrossRef]
33. Krishna, B.; Rao, Y.R.S.; Vijaya, T. Modelling groundwater levels in an urban coastal aquifer using artificial neural networks. *Hydrol. Process.* **2008**, *22*, 1180–1188. [CrossRef]
34. Nourani, V.; Mogaddam, A.A.; Nadiri, A.O. An ANN-based model for spatiotemporal groundwater level forecasting. *Hydrol. Process.* **2010**, *22*, 5054–5066. [CrossRef]
35. Kouziokas, G.N.; Chatzigeorgiou, A.; Perakis, K. Multilayer Feed Forward Models in Groundwater Level Forecasting Using Meteorological Data in Public Management. *Water Resour. Manag.* **2018**, *32*, 5041–5052. [CrossRef]
36. Rogers, L.L.; Dowla, F.U.; Johnson, V.M. Optimal field-scale groundwater remediation using neural networks and the genetic algorithm. *Environ. Sci. Technol.* **1995**, *29*, 1145–1155. [CrossRef]
37. Arndt, O.; Barth, T.; Freisleben, B.; Grauer, M. Approximating a finite element model by neural network prediction for facility optimization in groundwater engineering. *Eur. J. Oper. Res.* **2005**, *166*, 769–781. [CrossRef]
38. Bhattacharjya, R.K.; Datta, B. ANN-GA-based model for multiple objective management of coastal aquifers. *J. Water Resour. Plan. Manag.* **2009**, *135*, 314–322. [CrossRef]
39. Dhar, A.; Datta, B. Saltwater intrusion management of coastal aquifers. I: Linked simulation-optimization. *J. Hydrol. Eng.* **2009**, *14*, 1263–1272. [CrossRef]
40. Chau, K.; Wu, C.; Li, Y. Comparison of several flood forecasting models in Yangtze River. *J. Hydrol. Eng.* **2005**, *10*, 485–491. [CrossRef]
41. Dawson, C.W.; Wilby, R. An artificial neural network approach to rainfall-runoff modelling. *Hydrol. Sci. J.* **1998**, *43*, 47–66. [CrossRef]
42. Meng, C.; Zhou, J.; Tayyab, M.; Zhu, S.; Zhang, H. Integrating Artificial Neural Networks into the VIC Model for Rainfall-Runoff Modeling. *Water* **2016**, *8*, 407. [CrossRef]
43. Cheng, C.; Chau, K.W.; Sun, Y.; Lin, J. Long-Term Prediction of Discharges in Manwan Reservoir Using Artificial Neural Network Models. In *Proceedings of the Second International Conference on Advances in Neural Networks–Volume Part III*; Springer: Berlin/Heidelberg, Germany, 2005; pp. 1040–1045.
44. Taormina, R.; Chau, K.W.; Sethi, R. Artificial neural network simulation of hourly groundwater levels in a coastal aquifer system of the Venice lagoon. *Eng. Appl. Artif. Intell.* **2012**, *25*, 1670–1676. [CrossRef]
45. Mohanty, S.; Jha, M.K.; Kumar, A.; Sudheer, K.P. Artificial Neural Network Modeling for Groundwater Level Forecasting in a River Island of Eastern India. *Water Resour. Manag.* **2010**, *24*, 1845–1865. [CrossRef]
46. Afzaal, H.; Farooque, A.A.; Abbas, F.; Acharya, B.; Esau, T. Groundwater Estimation from Major Physical Hydrology Components Using Artificial Neural Networks and Deep Learning. *Water* **2019**, *12*, 5. [CrossRef]
47. Nayak, P.C.; Rao, Y.R.S.; Sudheer, K.P. Groundwater Level Forecasting in a Shallow Aquifer Using Artificial Neural Network Approach. *Water Resour. Manag.* **2006**, *20*, 77–90. [CrossRef]
48. Al-Senafy, M.; Abraham, J. Vulnerability of groundwater resources from agricultural activities in southern Kuwait. *Agric. Water Manag.* **2004**, *64*, 1–15. [CrossRef]

49. Van Camp, M.; Radfar, M.; Walraevens, K. Assessment of groundwater storage depletion by overexploitation using simple indicators in an irrigated closed aquifer basin in Iran. *Agric. Water Manag.* **2010**, *97*, 1876–1886. [CrossRef]
50. Giordano, R.; D'Agostino, D.; Apollonio, C.; Scardigno, A.; Pagano, A.; Portoghese, I.; Lamaddalena, N.; Piccinni, A.F.; Vurro, M. Evaluating acceptability of groundwater protection measures under different agricultural policies. *Agric. Water Manag.* **2015**, *147*, 54–66. [CrossRef]
51. Guangxin, Z.; Wei, D.; Lizhi, Z. Dynamic System Analysis and Control Countermeasures of Seawater Intrusion in Longkou City. *Environ. Pollut. Control-Hangzhou* **2001**, *23*, 317–319.

© 2020 by the authors. Licensee MDPI, Basel, Switzerland. This article is an open access article distributed under the terms and conditions of the Creative Commons Attribution (CC BY) license (http://creativecommons.org/licenses/by/4.0/).